Trace-element fractionation in plumes and the origin of HIMU mantle beneath the Cameroon line

Alex N. Halliday*, Jon P. Davidson*‡, Peter Holden*‡, Charles DeWolf*, Der-Chuen Lee* & J. Godfrey Fitton†

* Department of Geological Sciencies, University of Michigan, Ann Arbor, Michigan 48109-1063, USA
† Grant Institute of Geology, University of Edinburgh, West Mains Road, Edinburgh EH9 3JW, UK

The lavas of the Cameroon line display a lead isotope anomaly at the continent/ocean boundary which can be attributed to a fossil mantle plume, the diminishing lateral effects of which can be recognized as far as 400 km to either side. The high $^{206}Pb/^{204}Pb$ ratio—characteristic of the mantle endmember known as 'HIMU'—seems to arise from U/Pb fractionation accompanying melt migration following emplacement of the plume in the upper mantle 125 Myr ago.

MODELS for the genesis of ocean island basalts (OIB) can generally be divided into those invoking direct partial melting of plumes that have risen from below a thermal boundary layer separating the lower mantle from the convecting upper mantle (the latter generally thought to be the source of mid-ocean ridge basalts (MORB))[1-3], and those invoking preferential melting of relatively enriched components which are heterogeneously dispersed through the convecting upper mantle[4-7]. Isotope variations in the mantle are also commonly modelled in terms of different proportions of endmember components. The most clearly defined of these is characterized by very radiogenic Pb and unradiogenic Nd relative to Sr and has been variously referred to as the 'St Helena type' by White[8], the 'LoNd' type by Hart *et al.*[9] and the 'HIMU' type by Zindler and Hart[10]. Magmas of this nature (called HIMU in this paper) have been recognized in St Helena[11], Tubuaii[12-14], Mangaia[12,13], the Cameroon line[15,16], the Cape Verdes[17] and the Oslo Rift[18]. The HIMU component possesses special significance because it also represents the most extreme case of the 'lead paradox'[19] (the lead isotopic compositions of OIB and MORB imply that, relative to bulk Earth, their sources have time-integrated high U/Pb ratios, whereas a mantle source that has yielded melts should be characterized by low U/Pb because U is believed to be more incompatible than Pb). Explanations for the lead paradox generally, or for the HIMU component specifically, have included preferential partitioning of lead into the core for a significant period after accretion[20-22], recycling of ancient oceanic crust[2,8,12,13,17,23], delamination of sub-continental lithosphere[9,24,25], metasomatism by CO_2-rich fluids[13,26], preferential recycling back into the mantle of upper continental crust with the lower continental crust representing a repository of unradiogenic lead[27], and finally the possibility that lead is in fact more incompatible than uranium in mantle melting[28,29].

Studies of the volcanic rocks of the Cameroon line have played a useful part in constraining models for the genesis of OIB because of the unusual independent space-time constraints that can be applied to models of magma genesis[7,15,30,31]. Here we use these space-time constraints to demonstrate that HIMU characteristics were produced relatively recently in an upper-mantle plume as the time-integrated effect of trace-element fractionation between silicate minerals and melt, with U more incompatible than Pb.

The Cameroon line

The Cameroon line is a 1,600-km Y-shaped chain of volcanic centres and plutons extending northeast from the island of Pagalu in the Atlantic Ocean to the continental interior of west Africa (Fig. 1). There are 12 main volcanic centres, the products of which range in age from 30 Myr to the present[7]. In addition, there are 17 pluton complexes in the continental sector, which range in age from 65 to 30 Myr (refs 32, 33). It has been shown by isotope dating that there has been no systematic change in the focus of magmatism during this entire period[7]. Because the African plate has moved with respect to hotspots during the past 65 Myr (refs 34, 35), it is clear that the magmatic activity

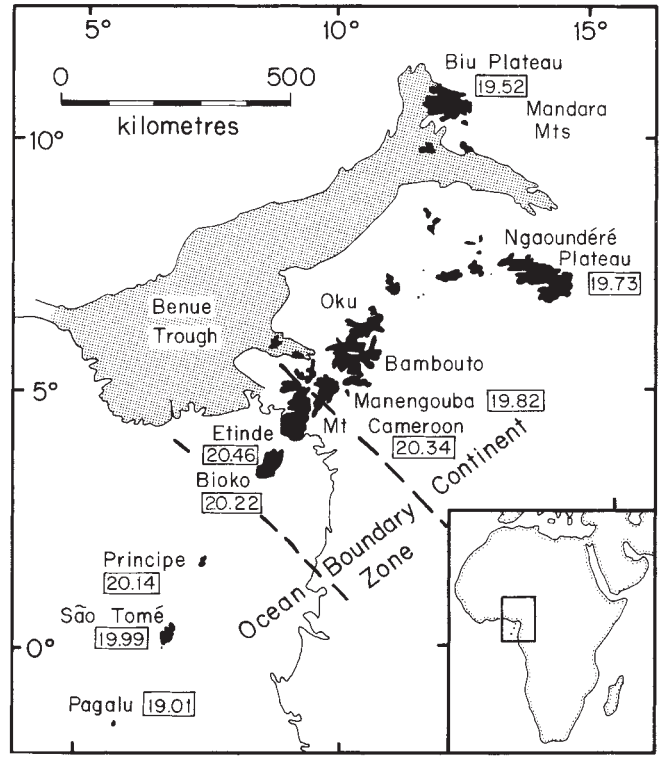

FIG. 1 Map of the area of the Cameroon line and the Gulf of Guinea showing the distribution of the main Cenozoic volcanic centres and the definition of the continent/ocean boundary region. The mean $^{206}Pb/^{204}Pb$ of the <10 Myr lavas is given for each locality. Data from Table 1 and refs 15 and 16.

‡ Present address: Department of Earth and Space Sciences, University of California, Los Angeles, California 90024, USA.

TABLE 1 Isotope and selected chemical data

Volcanic centre	Sample number	Age (Myr)	Lithology	Rb (p.p.m.)	Sr (p.p.m.)	Nd (p.p.m.)	$^{87}Sr/^{86}Sr$	$^{143}Nd/^{144}Nd$	ε_{Nd}	$^{206}Pb/^{204}Pb$	$^{207}Pb/^{204}Pb$	$^{208}Pb/^{204}Pb$
Manengouba	C55	3	Hy-normative basalt	36	636	46	0.70316 (3)	0.512957 (7)	+6.2	19.794	15.609	39.36
Manengouba	C69	1	Trachybasalt	62	788	60	0.70315 (2)	0.512923 (8)	+5.6	19.709	15.613	39.35
Manengouba	C51	1	Alkali basalt	37	757	46	0.70308 (2)	0.512929 (31)	+5.7	19.920	15.611	39.52
Manengouba	C59	1	Alkali basalt	37	945	56	0.70307 (1)	0.512904 (10)	+5.2	20.135	15.665	39.87
Manengouba	C72	1	Alkali basalt	43	918	54	0.70303 (1)	0.512867 (20)	+4.5	20.182	15.694	39.87
Manengouba	C70	1	Basanite	42	733	43	0.70300 (1)	0.512940 (9)	+5.9	19.634	15.625	39.27
Manengouba	C56	1	Hy-normative basalt	16	480	27	0.70299 (1)	0.512959 (10)	+6.3	19.572	15.652	39.30
Manengouba	C68	1	Hy-normative basalt	38	463	38	0.70298 (2)	0.512986 (13)	+6.8	19.795	15.635	39.50
Mt Cameroon	C201	0	Basanite	22	661	42	0.70339 (1)	0.512723 (7)	+1.7	19.983	15.620	39.84
Mt Cameroon	C201D	0	Diopside megacryst	1	74	8	0.70336 (2)	0.512758 (9)	+2.3	20.110	15.640	39.61
Mt Cameroon	C25	0	Basanite	36	989	70	0.70335 (1)	0.512777 (7)	+2.7	20.354	15.658	40.15
Mt Cameroon	C5	0	Tephrite	51	1,202	81	0.70328 (1)	0.512781 (8)	+2.8	20.375	15.655	40.15
Etinde	C24	0	Nephelinite	87	2,401	180	0.70337 (1)	0.512782 (2)	+2.8	20.455	15.662	40.31
Etinde	C150	0	Melanephelinite	89	1,054	85	0.70337 (2)	0.512800 (6)	+3.2	20.289	15.642	40.08
Etinde	C131	0	Hauyne nephelinite	349	2,825	86	0.70334 (1)	0.512809 (7)	+3.3	20.470	15.665	40.28
Etinde	C154	0	Nosean leucite nephelinite	201	6,553	41	0.70333 (1)	0.512835 (7)	+3.8	20.522	15.663	40.34
Etinde	C152	0	Hauyne nephelinite	114	2,395	142	0.70331 (1)	0.512804 (8)	+3.2	20.489	15.666	40.31
Bioko	FP32	0	Tephrite	61	1,199	79	0.70343 (1)	0.512769 (8)	+2.6	20.368	15.667	40.21
Bioko	FP1	0	Alkali basalt	26	726	47	0.70325 (1)	0.512839 (8)	+3.9	20.032	15.652	39.86
Bioko	FP23	0	Alkali basalt	26	685	55	0.70323 (2)	0.512843 (8)	+4.0	20.298	15.691	40.05
Bioko	FP38	0	Alkali basalt	25	647	43	0.70319 (1)	0.512860 (7)	+4.3	20.044	15.646	39.80
Principe	P16	6	Trachyphonolite	314	11	17	0.71092 (2)	0.512815 (9)	+3.5	20.224	15.674	39.80
Principe	P39	6	Phonolite	271	79	17	0.70378 (2)	0.512940 (8)	+5.9	20.259	15.677	39.80
Principe	P40	6	Phonolite	216	240	23	0.70328 (1)	0.512906 (8)	+5.2	20.285	15.673	39.82
Principe	P12	6	Tristanite	180	1,115	36	0.70322 (1)	0.512922 (10)	+5.5	20.226	15.680	39.86
Principe	P13	6	Tristanite	185	1,188	37	0.70301 (2)	0.512865 (20)	+4.4	20.237	15.701	39.93
Principe	P41	6	Trachyphonolite	174	484	27	0.70300 (1)	0.512930 (7)	+5.7	20.190	15.684	39.82
São Tomé	ST54	3	Trachyphonolite	213	468	20	0.70332 (2)	0.512853 (30)	+4.2	20.128	15.674	39.87
São Tomé	ST93	3	Hy-normative basalt	8	1,174	87	0.70320 (1)	0.512889 (10)	+4.9	20.064	15.666	39.79
São Tomé	ST72	3	Basanite	46	1,130	67	0.70318 (1)	0.512919 (6)	+5.5	19.997	15.683	39.72
São Tomé	ST43	1.3	Trachyte	129	463	46	0.70316 (1)	0.512937 (7)	+5.8	20.060	15.658	39.69
São Tomé	ST106	3	Alkali basalt	29	836	51	0.70315 (2)	0.512899 (21)	+5.1	19.944	15.653	39.56
São Tomé	ST100	3	Trachybasalt	139	1,204	39	0.70312 (1)	0.512925 (9)	+5.6	20.014	15.659	39.68
São Tomé	ST73	3	Tephrite	64	1,281	79	0.70307 (1)	0.512953 (7)	+6.1	20.074	15.720	39.80
São Tomé	ST110	3	Phonolitic tephrite	114	1,128	52	0.70299 (1)	0.512980 (10)	+6.7	20.124	15.691	39.84
São Tomé	ST109	3	Basanite	29	824	44	0.70299 (2)	0.512998 (7)	+7.0	19.954	15.676	39.57

Concentrations determined by X-ray fluorescence at University of Edinburgh. Isotope data determined at the Radiogenic Isotope Geochemistry Laboratory (University of Michigan) using techniques outlined elsewhere[55]. Errors refer to least significant digits and are 2σ mean run precisions. All isotopic ratios measured using a VG Sector multicollector mass spectrometer. Nd and Sr isotopic compositions were measured by multi-dynamic peak switching. Pb isotope data determined using static multicollection except C201D, measured with a Daly detector and ion counting. We obtain $^{87}Sr/^{86}Sr$ of 0.710242 (8) (2σ mean, $N=13$) for NBS987, and $^{143}Nd/^{144}Nd$ of 0.511855 (8) ($N=18$) for the La Jolla Nd standard. $^{87}Sr/^{86}Sr$ ratios are normalized to $^{86}Sr/^{88}Sr=0.1194$, and $^{143}Nd/^{144}Nd$ ratios are normalized to $^{146}Nd/^{144}Nd=0.7219$ with power-law fractionation corrections. Pb isotope data are corrected for fractionation and discrimination with a factor of 0.101% per a.m.u., based on measurements of the NBS981 standard. $\varepsilon_{Nd}=\{[(^{143}Nd/^{144}Nd)_{sample}/(^{143}Nd/^{144}Nd)_{bulk\,Earth}]-1\}\times10^4$. Bulk Earth $^{143}Nd/^{144}Nd=0.512638$, $^{147}Sm/^{144}Nd=0.1966$.

cannot be explained by conventional plume models (as have been advanced[36] to explain the Hawaiian hotspot trail, for example). Fitton and co-workers showed[7,30] that the average trace-element compositions of basalts in the Cameroon line were the same in continental and oceanic sectors, and argued that they were therefore derived from sub-lithospheric depths. A recent isotope study revealed, however, that lavas from the continent/ocean boundary region had relatively radiogenic lead, implying a genetic link with the lithosphere[15].

The isotope anomaly

Table 1 shows Nd, Sr and Pb isotope data for young (<10 Myr) samples of basalt, basanite, nephelinite and more evolved rocks from volcanic centres close to the continent/ocean boundary. The three volcanic centres at the continent/ocean boundary (Bioko, Etinde and Mt Cameroon) are distinctive, with radiogenic Pb and unradiogenic Nd for a given Sr isotopic composition relative to the 'mantle array' (Figs 2 and 3). In these respects the data are similar to the compositions observed for Cape Verdes, St Helena, Mangaia and Tubuaii[12–14,17], and therefore of the HIMU mantle type[10]. The anomaly straddles the continent/ocean boundary and is therefore not lithospheric contamination in the normal sense. This is supported by the data for diopside megacryst C201D and its host lava (C201), which have the least radiogenic Pb and Nd of the Mt Cameroon samples (Table 1). Slight contamination by old lithospheric components is a likely cause of such an effect (and for this reason these samples are ignored in further discussion) but clearly could not explain the overall very radiogenic Pb of the continent/ocean boundary lavas. Although the Pb isotope anomaly is most apparent in the three continent/ocean boundary volcanic centres, its effect can be observed in a progressively decreasing manner in the mean Pb isotopic compositions of younger lavas to either side of this zone (Fig. 1). Older Cameroon line lavas at a given locality tend to have less radiogenic lead[15]. Therefore to demonstrate clearly the magnitude of the geographical effect only analyses of young (<10 Myr) lavas are included in Table 1 and Fig. 1.

Plume models

The existence of a lead isotope anomaly in young lavas associated with an older lithospheric boundary underlines the inadequacy of conventional plume models for the Cameroon line (as with many rift-related magmatic provinces[37]) because the geometrical coincidence between a plume from the lower mantle and the continent/ocean boundary, which has moved with plate motions, would have to be accidental. A plausible explanation for the isotope anomaly is that the chemical and isotope characteristics of the magmas are inherited from the melting and/or assimilation of plume-modified mantle that has remained spatially fixed relative to the lithosphere since the formation of the Gulf of Guinea[15]. This mantle would have been a mixture of asthenospheric mantle, excavated older subcontinental lithosphere, and components from a newly rising plume, which had already been instrumental in the formation of the continent/ocean boundary.

At the time of opening of the south Atlantic, the region occupied by the present continent/ocean boundary in the vicin-

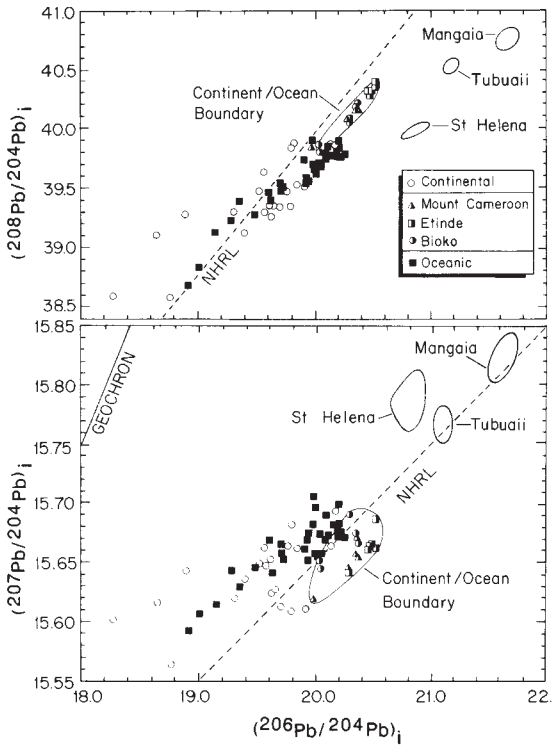

FIG. 2 Plot of initial Pb isotope data for the volcanic rocks of the Cameroon line, in the context of other HIMU (LoNd) types. Data from Table 1, refs 15, 16 and unpublished data for older lavas.

ity of the Gulf of Guinea (Fig. 1) overlay the St Helena hotspot[35]. The idea that the St Helena plume was instrumental in the breakup of Africa, the transfer of HIMU components into the upper mantle and the resultant location of a (diluted) Pb isotope anomaly along the Cameroon line is therefore appealing[15]. The data presented here indicate that such a plume affected the surrounding mantle over a radius of some 400 km. This is similar to the size of plume heads envisaged by White and McKenzie[38].

Schilling and co-workers[39,40] have demonstrated the lateral effects of hotspots on the Mid-Atlantic Ridge and attributed such effects to large-scale lateral flow towards the ridge. In the case of the Cameroon line it is clear that unless the relationship between the hotspots and the continent/ocean boundary is accidental rather than genetic, the general symmetry and apex of the hypothesized plume has been preserved in its original location in the uppermost mantle for 125 Myr. The Cameroon line data cannot be explained by models of redistribution of heterogeneities by large-scale lateral flow in the asthenosphere.

The generation of plume-like anomalies

Despite the apparent elegance of a fossil-plume model and the general similarities between St Helena and Cameroon isotopic compositions, there are problems with this interpretation. The Pb isotope data for the St Helena volcanic rocks are in fact distinct from those of the Cameroon line, and the differences cannot easily be reconciled by hypothesizing different proportions of the same plume component mixed with other Cameroon line compositions. The St Helena volcanic rocks display lower $^{208}Pb/^{204}Pb$ and higher $^{207}Pb/^{204}Pb$ (Fig. 2). The κ_{Pb} values (the time-integrated Th/U ratios deduced from the Pb isotope data[41]) for the continent/ocean boundary samples are consistently 3.9 to 4.0, compared with the values of ~3.7 for St Helena[41]. Furthermore, although showing the same effect of displacement below the 'mantle array', the Nd and Sr isotopic compositions do not lie on a mixing trajectory from the other Cameroon line data towards the field for St Helena (Fig. 3).

A significant feature of the lead isotope data for the continent/ocean boundary samples is that the range in $^{207}Pb/^{204}Pb$ is relatively uniform between different volcanic centres and displays no special distinction from the data for the rest of the Cameroon line; it is only the $^{206}Pb/^{204}Pb$ and $^{208}Pb/^{204}Pb$ ratios that are especially high (Fig. 2). This is illustrated in Fig. 4 where the different centres can be seen to define a series of sub-parallel arrays on a plot of $^{207}Pb/^{204}Pb$ against $^{206}Pb/^{204}Pb$. The slopes of these arrays correspond to apparent ages of roughly 1 Gyr. Such parallel arrays cannot be easily explained as offsets produced by different degrees of mixing between two heterogeneous components with a similar range in $^{207}Pb/^{204}Pb$ (although clearly this could have enhanced the scatter) because each volcanic centre seems to be relatively restricted in its range of $^{206}Pb/^{204}Pb$. Neither can they represent a variety of mixing lines between a radiogenic lead component with high $^{207}Pb/^{204}Pb$ and a range of different components with less radiogenic and variable $^{206}Pb/^{204}Pb$ ratios because the plot of $^{208}Pb/^{204}Pb$ against $^{206}Pb/^{204}Pb$ displays a tight collinear trend for virtually all of the Cameroon line samples (Fig. 2*a*). The offsets between different volcanic centres displayed in Fig. 4 are most simply explained as the result of relatively recent variable enrichment in the U/Pb and Th/Pb ratios. This has the effect of producing correlated offsets in $^{206}Pb/^{204}Pb$ and $^{208}Pb/^{204}Pb$, with little change in $^{207}Pb/^{204}Pb$, because of the much longer half-lives of ^{238}U and ^{232}Th relative to ^{235}U. Such a process is easily modelled as shown in Fig. 4, assuming that the last major fractionation event took place at 125 Myr when the Gulf of Guinea (hence continent/ocean boundary) formed. The lead isotope data themselves merely indicate young trace-element fractionation; it is the coincidence and inferred genetic link with the continent/ocean boundary that form the basis for proposing the exact timing as 125 Myr. The general magnitudes of $^{238}U/^{204}Pb$ and $^{232}Th/^{238}U$ (approximately equal to Th/U) ratios required to generate the range of modelled lead isotopic compositions are also indicated on Fig. 4. How realistic these values are can be assessed in part by comparisons with measured U/Pb ratios for the lavas themselves. Table 2 provides new isotope-dilution data for U, Pb, Sm and Nd in lavas from the three continent/ocean boundary volcanic centres. The average measured $^{238}U/^{204}Pb$ ratios are generally similar to the modelled values in Fig. 4 and they increase in the order Bioko, Mt Cameroon, Etinde, as predicted by the model.

Implicit in this model is the generally held assumption (recently challenged by Meijer and co-workers[28,29] who have argued the opposite as an explanation for the lead paradox)

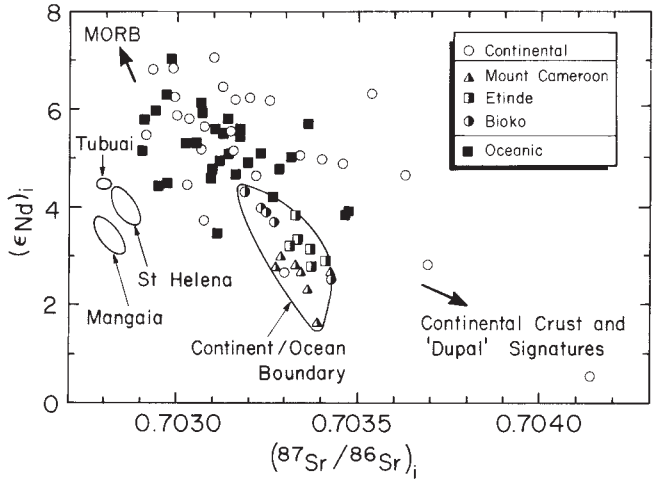

FIG. 3 Plot of initial ε_{Nd} against initial $^{87}Sr/^{86}Sr$ for volcanic rocks of the Cameroon line, in the context of other HIMU (LoNd) types. Data from Table 1, refs 15, 16 and unpublished data for older lavas.

TABLE 2 Sm, Nd, U and Pb concentrations

Locality	Sample number	Sm (p.p.m.)	Nd (p.p.m.)	$^{147}Sm/^{144}Nd$	U (p.p.m.)	Pb (p.p.m.)	$^{238}U/^{204}Pb$
Bioko	FP1	9.67	45.6	0.1282	1.07	2.76	25.7
	FP38	8.79	40.5	0.1311	0.775	2.54	20.2
Etinde	C24	25.1	17.6	0.08613	5.68	7.66	49.8
	C150	14.3	89.6	0.09662	2.45	3.84	42.6
Mount Cameroon	C201	7.72	43.0	0.1085	1.25	2.41	34.3
	C25	11.9	68.9	0.1043	2.13	3.75	38.0

Concentrations determined by isotope dilution.

that U is a more incompatible element than Pb in mantle melting. This can be substantiated using the Cameroon line data. Figure 5*a* shows that there is a general positive correlation between lead isotopic composition and measured $^{238}U/^{204}Pb$ ratio of the more primitive Cameroon line basalts, the slope of which is consistent with a model of young growth of radiogenic lead in the mantle. This relationship suggests that the $^{238}U/^{204}Pb$ ratio of the lavas is a function of the ratio in the source. Figure 5*b*, *c* shows that the U concentration increases, and the Sm/Nd ratio decreases, with increasing U/Pb ratio, consistent with U being more incompatible than Pb in these magmas. The simplest explanation for a relationship between U/Pb, Nd/Sm and $^{206}Pb/^{204}Pb$ ratio is that these ratios are correlated in the sources of the magmas. These data, together with those for other basalts, support the view[42] that U is more incompatible than Pb in mantle melting and that the fractionation in U/Pb ratios (as with Sm/Nd ratios) is dominantly controlled by silicate mineral/melt equilibria, rather than by sulphide or metal phases (see ref. 29).

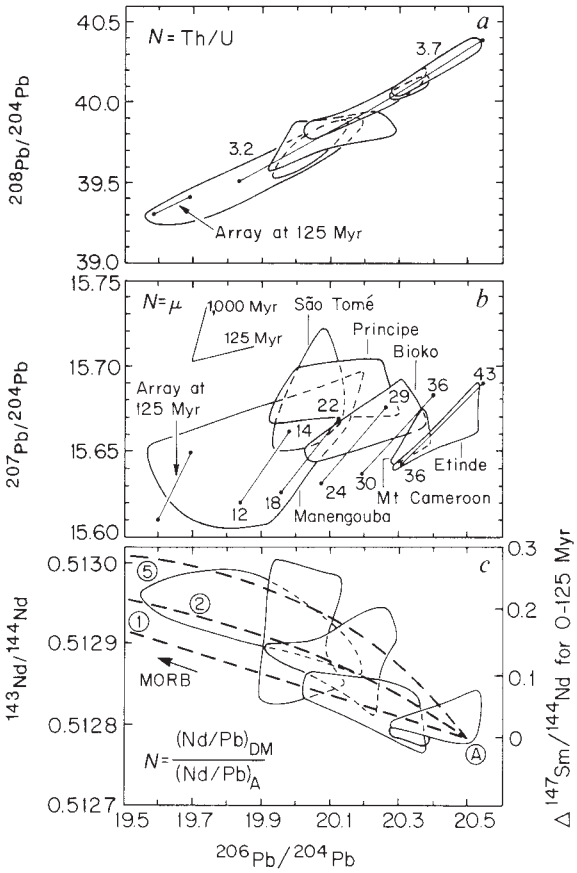

FIG. 4 Pb and Nd isotope data for young (<10 Myr) lavas of the Cameroon line divided according to volcanic centres. The Pb isotope differences between the volcanic centres are explicable if there has been relatively recent fractionation of the U/Pb ratios which will have a greater effect on the $^{206}Pb/^{204}Pb$ ratio than the $^{207}Pb/^{204}Pb$ ratio. The lines in *a* and *b* are model Pb isotope arrays produced from an initial linear array at 125 Myr (shown at the left) using the different $^{238}U/^{204}Pb$ and $^{232}Th/^{238}U$ values indicated. The model assumes that the $^{238}U/^{204}Pb$ and $^{232}Th/^{238}U$ values are proportional to each other and to variations in the $^{238}U/^{204}Pb$ and $^{232}Th/^{238}U$ values that produced the original array. *c* shows the relationship between the Pb and Nd isotopic compositions and the considerable $^{147}Sm/^{144}Nd$ variation necessary to account for the Nd isotope variations purely by radioactive decay over the past 125 Myr. An explanation for the large variation in Nd isotopic composition is that the magmas farther away from the continent/ocean boundary include components from depleted (MORB-like) sources. This is modelled with mixing curves constructed for different values of *N* (circled). Data from Table 1, and refs 15 and 16.

A consequence of the inverse relationship between U/Pb and Sm/Nd fractionation is that increased source U/Pb ratios toward the continent/ocean boundary should be accompanied by decreased Sm/Nd ratios and therefore relatively unradiogenic Nd as shown in Fig. 3. Figure 4 shows the relationship between $^{206}Pb/^{204}Pb$ ratios and the Nd isotopic compositions of the young volcanic rocks of the Cameroon line. The general trends of the data are consistent with our model, but for the variations in Nd and Sr isotopic composition to be generated entirely by radioactive decay over 125 Myr requires source variations of 0.2 in both $^{147}Sm/^{144}Nd$ and $^{87}Rb/^{86}Sr$. Given the range in U/Pb, Rb/Sr and Sm/Nd measured in the spectrum of OIB and pristine MORB glasses[15,42,43], the modelled source parent/daughter ratios are not impossible, although extreme, particularly for Sm/Nd. The most likely explanation for this is that the lavas from farther away from the continent/ocean boundary have inherited components from more depleted mantle with high Nd/Pb and Sr/Pb ratios such as MORB sources. This explanation is supported by the modelled curvature of the data arrays toward a depleted mantle component with high Nd/Pb (Fig. 4). Such a model is further supported by the relatively unradiogenic lead isotopic compositions of the more distant Cameroon line volcanic centres of Pagalu, Biu and Ngaoundéré[15].

Plume differentiation and interaction

Recent attempts to model the fluid dynamics of plumes and thermals[44-48] have shown that such bodies may rise by a combination of shear flow and entrainment of the surrounding mantle, resulting in incorporation and circulation of components from the ambient mantle in the plume head itself. As a result, the compositional outline of the plume head may develop a 'doughnut shape', with a core of contaminated material. This has the interesting effect that the mantle in the core of the head should not be as enriched as that occupying the region immediately to either side (assuming that the plume is trace-element enriched relative to the ambient mantle)—which should produce a widely spaced pair of anomalies to either side of the plume axis, quite unlike the pattern shown in Fig. 1. We propose instead that the magmas are derived by remelting of a fossil plume, and that the isotope anomaly observed towards the central portions of the Cameroon line, reflects the time-integrated effect of trace-element fractionation during melt migration in the plume head as it cooled after emplacement at 125 Myr. We suggest that the Cameroon line magmas are currently derived from a zone in

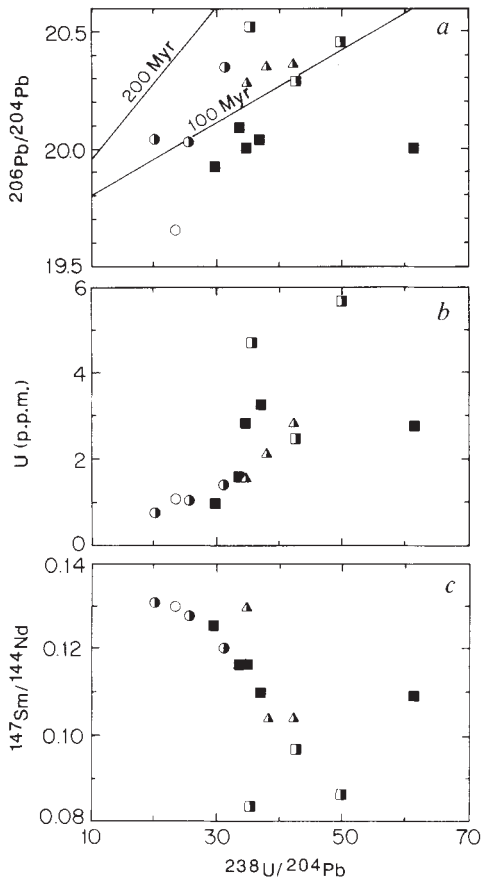

FIG. 5 Relationship betweeen the $^{238}U/^{204}Pb$ and *a*, $^{206}Pb/^{204}Pb$, *b*, U concentration and *c*, $^{147}Sn/^{144}Nd$ for the young (<10 Myr) Cameroon line lavas with >4 wt% MgO from the volcanic centres in Table 1. These relationships are easily explained if U is more incompatible than Pb and U/Pb (like Sm/Nd) is controlled by silicate solid/liquid partitioning in the magma sources. The one oceanic sample with anomalously high $^{238}U/^{204}Pb$ is a nephelinite from Principe. Data from Tables 1 and 2, and refs 15, 16.

the upper portions of the fossil plume, enriched by basaltic melts that percolated upward during compaction of the head (Fig. 6). The degree of trace-element enrichment (hence U/Pb ratio) in this zone, would then increase laterally towards the centre, as a function of the vertical thickness of relatively enriched mantle (the flattened plume head) through which the melts migrated during plume compaction. At the margins, where the flattened plume is thinnest, the source regions are dominated by more depleted mantle (Fig. 6), as reflected in the change in Nd, Sr and Pb isotopic compositions towards either end of the Cameroon line, culminating in the highly depleted isotopic compositions observed for centres like Pagalu.

Trace-element fractionation

The Pb isotopic compositions for the three continent/ocean boundary centres imply source U/Pb minima of 0.152 for Etinde and 0.033 for Mt Cameroon, based on the differences with Bioko, assuming closed-system evolution over 125 Myr. The Th/U ratio of the source of these three volcanoes can be estimated at ~3.3 (from the slope of the data in Fig. 2*a*). Although this is probably a slight overestimate[49] it is consistent with the modelling in Fig. 4, and is intermediate between the Cameroon line κ_{Pb} values (3.9–4.0) and the κ_{Th} values of MORB (2.5) (ref. 41). These U/Pb and Th/U estimates, together with the model estimates shown in Fig. 4, provide evidence that the upper-mantle sources are more enriched than MORB sources (in contrast to some models for OIB[7]).

The minimum U/Pb ratio measured for the lavas can be compared with that estimated for the sources based on time-integrated differences, to derive a value for the maximum fractionation in U/Pb ratio (4) during production of the continent/ocean boundary magmas. The U/Pb fractionation required to generate the range in lead isotopic compositions is less than five. U/Pb fractionations in this range can easily be achieved with fractional melting[50,51], and bulk (solid/liquid) distribution coefficients for U and Pb that are within a factor of about six of each other, assuming a constant melt fraction in contact with solid of 0.01, and fractions of melt removed of between 0.01 and 0.10. The U/Pb fractionations hypothesized for both 125 Myr and during the melting that produced the young Cameroon line magmas, are therefore reasonable given the range of experimental silicate mineral/melt U and Pb partition coefficients[52,53], and do not require special CO_2 metasomatism or phases other than silicates.

The reasonably common occurrence of basalts with HIMU isotope characteristics is evidence that the fractionation processes that took place during melting in the mantle under the Cameroon line may not be unusual. Obviously such fractionations do not have to be recent as in the case of the Cameroon line (the St Helena $^{207}Pb/^{204}Pb$ ratios cannot be explained by the model of recent fractionation presented here). Nevertheless an important implication of the large range in parent/daughter ratios measured and modelled here is that they will generate mantle that is extremely heterogeneous isotopically if allowed to evolve over long periods of time (gigayears). Although such an effect is well illustrated by storage in the sub-continental lithosphere[54], the relative homogeneity of MORB and to a lesser extent OIB compositions[43] implies that heterogeneities produced from small amounts of partial melting are destroyed or greatly diluted in the long-term cycling of the convecting mantle. In these respects our data are consistent with the evidence for short residence times for lead in the upper mantle presented by Galer and O'Nions[41].

Although the Cameroon line plume was apparently already relatively enriched when it was introduced into the upper mantle at 125 Myr, the high κ_{Pb} values for the Cameroon line are difficult to reconcile with models that explain this enrichment in terms of recycling of uranium-enriched (low Th/U) altered oceanic crust into the deep mantle (such as is more readily applied to the data for St Helena, for example). If trace-element fractionation by melting in the mantle produces Nd–Sr isotope data that are below the mantle array and can be taken to the

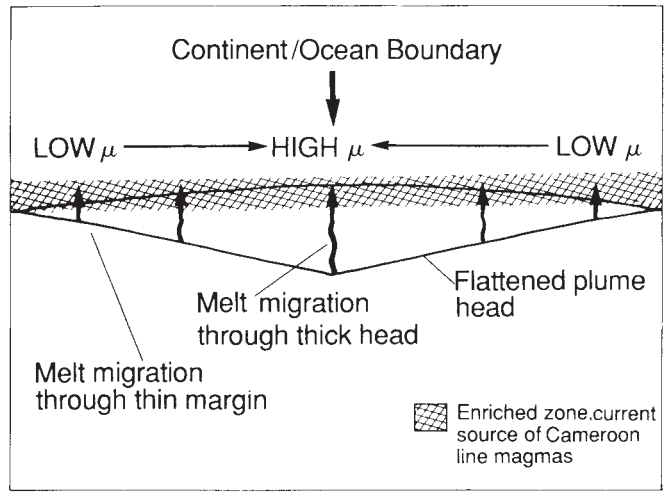

FIG. 6 Cartoon illustrating model for source enrichment following plume emplacement at 125 Myr.

extreme of explaining all HIMU components, the case for a distinctive isotope signature for ancient recycled oceanic crust may need re-evaluating. Conversely the best explanation for the mantle array itself may be recycling, rather than melt fractionation[10,11]. Regardless of these possibilities, this study shows that HIMU mantle can simply represent the time-integrated consequence of storage of small-degree partial melts in the upper mantle and, contrary to recent suggestions, the lead paradox is not resolvable simply in terms of U and Pb partitioning during melting. □

Received 9 July; accepted 23 August 1990.

1. Allègre, C. J. *Tectonophysics* **81,** 109-132 (1982).
2. Hofmann, A. W. & White, W. M. *Earth planet. Sci. Lett.* **57,** 421-436 (1982).
3. Storey, M. *et al. Nature* **336,** 371-374 (1988).
4. Morris, J. D. & Hart, S. R. *Geochim. cosmochim. Acta* **47,** 2015-2030 (1983).
5. Sleep, N. H. *J. geophys. Res.* **89,** 10029-10041 (1984).
6. Zindler, A., Staudigel, H. & Batiza, R. *Earth planet. Sci. Lett.* **70,** 175-195 (1984).
7. Fitton, J. G. & Dunlop, H. M. *Earth planet. Sci. Lett.* **72,** 23-38 (1985).
8. White, W. M. *Geology* **13,** 115-118 (1985).
9. Hart, S. R., Gerlach, D. C. & White, W. M. *Geochim. cosmochim. Acta* **50,** 1551-1557 (1986).
10. Zindler, A. & Hart, S. *A. Rev. Earth planet. Sci.* **14,** 493-571 (1986).
11. White, W. M. & Hofmann, A. W. *Nature* **196,** 821-825 (1982).
12. Palacz, Z. A. & Saunders, A. D. *Earth planet. Sci. Lett.* **79,** 270-280 (1986).
13. Nakamura, Y. & Tatsumoto, M. *Geomochim. cosmochim. Acta.* **52,** 2909-2924 (1988).
14. Vidal, Ph., Chauvel, C. & Brousse, R. *Nature* **307,** 536-538 (1984).
15. Halliday, A. N., Dickin, A. P., Fallick, A. E. & Fitton, J. B. *J. Petrol.* **29,** 181-211 (1988).
16. Fitton, J. G., Kilburn, C. R. J., Thirlwall, M. F. & Hughes, D. J. *Nature* **306,** 327-332 (1983).
17. Gerlach, D. C., Cliff, R. A., Davies, G. R., Norry, M. & Hodgson, N. *Geochim. cosmochim. Acta* **52,** 2979-2992 (1988).
18. Anthony, E. Y., Segalstad, T. V. & Neuman, E-R. *Geochim. cosmochim. Acta* **53,** 1067-1076 (1989).
19. Allègre, C. J. *Earth planet. Sci. Lett.* **5,** 261-269 (1969).
20. Vidal, P. & Dosso, L. *Geophys. Res. Lett.* **5,** 169-172 (1978).
21. Vollmer, R. *Nature* **270,** 144-147 (1977).
22. Allègre, C. J., Dupre, B. & Brevart, O. *Phil. Trans. R. Soc.* A**306,** 49-59 (1982).
23. Chase, C. G. *Earth planet. Sci. Lett.* **52,** 277-284 (1981).
24. McKenzie, D. & O'Nions, R. K. *Nature* **301,** 229-231 (1983).
25. O'Nions, R. K. *J. geol. Soc., Lond.* **144,** 259-274 (1987).
26. Menzies, M. A. & Wass, S. Y. *Earth planet. Sci. Lett.* **65,** 287-302 (1983).
27. O'Nions, R. K., Evensen, N. M. & Hamilton, P. J. *J. geophys. Res.* **84,** 6091-6101 (1979).
28. Meijer, A. *Geophys. Res. Lett.* **12,** 741-744 (1985).
29. Meijer, A., Kwon, T-T. & Tilton, G. R. *J. geophys. Res.* **95,** 433-448 (1990).
30. Fitton, J. G. *Spec. Publs geol. Soc. Lond.* **30,** 273-291 (1987).
31. Dunlop, H. M. & Fitton, J. G. *Contr. Miner. Petrol.* **71,** 125-131 (1979).
32. Lasserre, M. *Bull. Bur. Rech. geol. min. Paris* 2e Ser., Sect. IV, No. 2, 143-159 (1978).
33. Cantagrel, J-M., Jamond, C. & Lasserre, M. *C. r. somm. Soc. geol. Fr.* **6,** 300-303 (1978).
34. Morgan, J. W. *Tectonophysics* **94,** 123-139 (1983).
35. Fitton, J. G. *Earth planet. Sci. Lett.* **51,** 132-138 (1980).
36. Dalrymple, G. B., Clague, D. A., Garcia, M. O. & Bright, S. W. *Bull. geol. Soc. Am.* **92,** 315-318 (1981).
37. Phipps, S. P. *Nature* **334,** 27-31 (1988).
38. White, R. & McKenzie, D. *J. geophys. Res.* **94,** 7685-7729 (1989).
39. Schilling, J-G. *Nature* **314,** 62-67 (1985).
40. Schilling, J-G., Thompson, G., Kingsley, R. & Humphris, S. *Nature* **313,** 187-191 (1985).
41. Galer, S. J. G. & O'Nions, R. K. *Nature* **316,** 778-782 (1985).
42. Newsom, H. E., White, W. M. Jochum, K. P. & Hofmann, A. W. *Earth planet. Sci. Lett.* **80,** 299-313 (1986).
43. Cohen, R. S. & O'Nions, R. K. *J. Petrol.* **23,** 299-324 (1982).
44. Griffitths, R. W., Gurnis, M. & Eitelberg, G. *Geophys. J.* **96,** 477-495 (1989).
45. Olson, P. & Singer, H. *J. Fluid Mech.* **158,** 511-531 (1985).
46. Griffiths, R. W. *Earth planet. Sci. Lett.* **78,** 435-446 (1986).
47. Griffiths, R. W. *Phys. Earth planet. Inter.* **43,** 261-273 (1986).
48. Griffiths, R. W. *J. Fluid Mech.* **166,** 115-138 (1986).
49. White, W. M., Hofmann, A. W. & Puchelt, H. *J. geophys. Res.* **92,** 4881-4893 (1987).
50. McKenzie, D. *Earth planet. Sci. Lett.* **74,** 81-91 (1985).
51. Langmuir, C. H., Bender, J. F., Bence, A. E. & Hanson, G. N. *Earth planet. Sci. Lett.* **36,** 133-156 (1977).
52. Seitz, M. G. *Yb Carnegie Instn Wash.* **72,** 551-553 (1973).
53. Watson, E. B., Ben Othman, D., Luck, J-M. & Hofmann, A. W. *Chem. Geol.* **62,** 191-208 (1987).
54. Vollmer, R. & Norry, M. J. *Nature* **301,** 141-143 (1983).
55. Halliday, A. N. *et al. Earth planet. Sci. Lett.* **94,** 274-290 (1989).

ACKNOWLEDGEMENTS. We thank R. Keller and M. Johnson for technical help, S. Djallo, R. Temdjim, G. Davies, M. Gurnis and K. Mezger for discussions, and W. White and A. Saunders for review. This work was supported by the Turner Fund (University of Michigan) and the NSF (A.N.H.) and by NERC (J.G.F.).

Dwarf locus mutants lacking three pituitary cell types result from mutations in the POU-domain gene *pit-1*

Sen Li*†, E. Bryan Crenshaw III*, Elizabeth J. Rawson*, Donna M. Simmons‡§, Larry W. Swanson‡§ & Michael G. Rosenfeld*§

* Eukaryotic Regulatory Biology Program, † Department of Chemistry, and § Howard Hughes Medical Institute, School of Medicine, M-013, University of California, San Diego, La Jolla, California 92093, USA
‡ Neural Systems Laboratory, The Salk Institute, La Jolla, California 92037, USA

Mutations at the mouse dwarf locus (*dw*) interrupt the normal development of the anterior pituitary gland, resulting in the loss of expression of growth hormone, prolactin and thyroid-stimulating hormone, and hypoplasia of their respective cell types. Disruptions in the gene encoding the POU-domain transcription factor, Pit-1, occur in both characterized alleles of the dwarf locus. The data indicate that Pit-1 is necessary for the specification of the phenotype of three cell types in the anterior pituitary, and directly link a transcription factor to commitment and progression events in mammalian organogenesis.

ANALYSES of developmental *Drosophila* and *Caenorhabditis elegans* mutants[1-4] suggest models in which sequential activation of a hierarchy of regulatory genes dictates the temporal and spatial patterns of the expression of gene products that define cell phenotypes. Similarly, organogenesis in mammals results from the ordered expression of cell phenotypes and, presumably, is also determined by the sequential activation of regulatory genes. The development of the anterior pituitary gland provides an excellent model system in which to study cell-specific gene activation and the processes by which distinct cell types develop within an organ. The anterior pituitary arises from a placode in Rathke's pouch, derived from the somatic ectoderm[5]. The five phenotypically distinct cell types appear in a stereotypical order with the growth hormone-producing somatotrophs and the prolactin-producing lactotrophs being the last two cell types to appear[1-7].

The cell-specific expression of the rat prolactin and growth hormone genes depends on synergistic interactions between *cis*-active elements[8-16]. A pituitary-specific transcription factor, Pit-1, binds to these elements in both genes and can transactivate prolactin and growth hormone gene promoters both *in vitro* and in cell transfection experiments (refs 17-20, R. Maurer & D. Sharp personal communication), although one group[21] found that Pit-1 binds only to the growth hormone gene promoter. The